MATERIALS SCIENCE

Uniform hierarchical MFI nanosheets prepared via anisotropic etching for solution-based sub–100-nm-thick oriented MFI layer fabrication

Yi Liu[1], Weili Qiang[1], Taotao Ji[1], Mu Zhang[1], Mingrun Li[2], Jinming Lu[1], Yi Liu[1]*

Zeolite nanosheets have shown unprecedented opportunities for a wide range of applications, yet developing facile methods for fabrication of uniform zeolite nanosheets remains a great challenge. Here, a facile approach involving anisotropic etching with an aqueous solution of tetrapropylammonium hydroxide (TPAOH) was developed for preparing uniform high–aspect ratio hierarchical MFI nanosheets. In addition, the mechanism associated with the formation of MFI nanosheets was proposed. In the next step, a dynamic air-liquid interface–assisted self-assembly method and single-mode microwave heating were used for *b*-oriented MFI nanosheets monolayer deposition and controlled in-plane solution-based epitaxial growth, respectively, ensuring the formation of well-intergrown *b*-oriented MFI layers with sub–100-nm thickness. Moreover, our study indicated that *b*-oriented ultrathin MFI layers could be fabricated on diverse substrates demonstrating excellent anticorrosion capacity, ionic sieving properties, and *n*-/*i*-butane isomer separation performance.

INTRODUCTION

The emergence of two-dimensional zeolite nanosheets (NSs) opens up unprecedented opportunities for promoting their adsorption, catalytic, and separation performances due to the reduced diffusion path lengths, increased surface areas, and enhanced surface activity compared with their bulky counterparts (*1*–*4*). Among these applications, the use of zeolite NSs as building blocks for the fabrication of oriented ultrathin zeolite layers represents an important research direction demonstrating the microstructural benefits of zeolite NSs (*5*–*10*). As far as MFI-type zeolites are concerned, fabrication of *b*-oriented MFI zeolite layers, which has proven effective in reducing internal diffusion barriers and grain boundary defects (*11*), generally involves preparation of regularly shaped MFI seeds (*12*), *b*-oriented deposition of MFI seeds on substrates (*13*–*15*), and subsequent in-plane epitaxial growth (*16*, *17*). In comparison with conventional coffin-shaped MFI crystals, microstructural benefits derived from MFI NSs seeds such as the high aspect ratio and short diffusion path length along the *b* axis greatly facilitated precise control over both orientation and thickness of MFI layers (*7*, *18*).

Diverse methods have recently been developed for the preparation of MFI NSs with varying microstructures (*1*, *6*, *7*). For instance, Tsapatsis prepared 3- to 5-nm-thick high–aspect ratio MFI NSs by top-down exfoliation of multilamellar MFI precursors or bottom-up single rotational intergrowth-triggered nanocrystal-seeded growth (*6*, *7*, *19*), while Hedlund prepared hydrophobic 10-nm-thick MFI crystals by long-term aging in fluoride medium (*20*). Recently, Xiao studied formation energies of SAPO-11 zeolite NSs with varying unit-cell layers by theoretical calculations and concluded that 12 unit-cell-thick zeolite NSs had a crystal energy comparable with bulk crystals (*21*). Therefore, it was expected that the use of ca. 12 unit-cell-thick (equivalent to ca. 25 nm thick along the *b* axis) MFI NSs having high aspect ratios as seeds would achieve a better balance between phase stability and diffusion barrier.

Besides thickness control of MFI seeds, recent decades witnessed notable progress in thickness control of *b*-oriented MFI layers during in-plane epitaxial growth (*20*, *22*–*24*). For instance, Tsapatsis and Hedlund reported the successful fabrication of 12- and 36-nm-thick *b*-oriented MFI films on silicon wafers and glass plates via gel-less (*23*) and dry-gel conversion methods (*20*), respectively. Compared with other methods, solution-based epitaxial growth may show superiority in terms of nutrient distribution uniformity and reaction condition mildness. Nevertheless, to date, there has been no report on the preparation of sub–100-nm-thick MFI layers via solution-based epitaxial growth. Recently, Tsapatsis synthesized 300-nm-thick *b*-oriented MFI films via solution-based epitaxial growth of 5-nm-thick MFI NSs monolayers on Si wafers (*25*). To prepare sub–100-nm-thick *b*-oriented MFI layers with few twins, a more efficient heating method enabling precise thickness control must be developed.

Motivated by the above concerns, here we developed a progressive wall-thinning approach for facile preparation of ca. 12 unit-cell-thick MFI NSs with high uniformity and high aspect ratio. After *b*-oriented deposition of MFI NSs monolayers, sub–100-nm-thick *b*-oriented MFI layers were further prepared via solution-based epitaxial growth. The rational design of qualified MFI NSs seeds, the employment of a dynamic air-liquid interface–assisted self-assembly (DALIAS) method for oriented deposition of MFI NSs, and the use of single-mode microwave heating during solution-based epitaxial growth were found crucial for exerting precise control over their thickness (Fig. 1). To the best of our knowledge, this represents the first report of the fabrication of sub–100-nm-thick oriented zeolite layers via solution-based epitaxial growth. In addition, with this method, we successfully prepared *b*-oriented ultrathin MFI layers on diverse substrates including smooth glass plates, coarse Al plates, inert Pt electrodes, and porous γ-Al_2O_3 substrates showing excellent anticorrosion capacity, ionic sieving properties, and *n*-/*i*-butane isomer separation performance, respectively.

[1]State Key Laboratory of Fine Chemicals, School of Chemical Engineering, Dalian University of Technology, Linggong Road NO. 2, Ganjingzi District, Dalian 116024, China. [2]State Key Laboratory of Catalysis, Dalian Institute of Chemical Physics, Chinese Academy of Sciences, Zhongshan Road NO. 457, Shahekou District, Dalian 116023, China.
*Corresponding author. Email: diligenliu@dlut.edu.cn

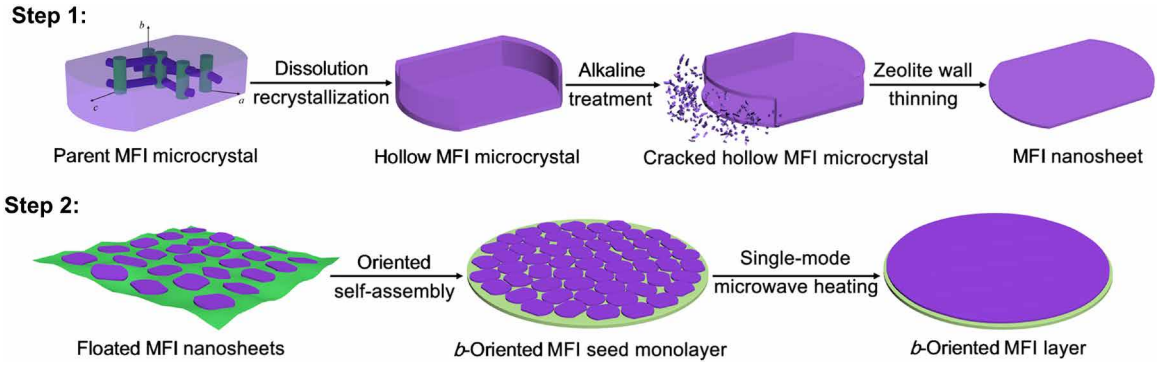

Fig. 1. Procedure for the preparation of sub–100-nm-thick *b*-oriented MFI layers by combining (1) NSs preparation and (2) MFI layer fabrication.

RESULTS

Synthesis of MFI NSs

The first step involves facile preparation of MFI NSs. Parent MFI crystals, which were synthesized by a simple hydrothermal method (*26*), exhibited uniform coffin-shaped morphology (0.9 μm × 0.45 μm × 1.2 μm; Fig. 2A). Subsequent hydrothermal treatment of calcined parent MFI crystals with aqueous tetrapropylammonium hydroxide (TPAOH) solution resulted in the formation of ca. 25-nm-thick MFI NSs with high uniformity and high aspect ratios (ca. 50) under optimized hydrothermal conditions (Fig. 2, B and C). Atomic force microscope (AFM) height image (Fig. 2D) indicated that the average thickness of MFI NSs was ~25 nm along the *b* axis. X-ray diffraction (XRD) patterns further confirmed the high purity and crystallinity of the obtained MFI NSs (Fig. 2E). In addition, transmission electron microscopy (TEM) and Brunauer-Emmett-Teller (BET) analyses were further carried out to investigate their mesoscopic structures. TEM results (Fig. 2F) indicated that there existed substantial mesopores inside MFI NSs maintaining a single-crystal structure of MFI type (shown in fig. S1), while BET results illustrated that calcined MFI NSs exhibited a typical type IV isotherm (fig. S2A) featuring a hierarchical pore structure centering at 2.8 nm (fig. S2, B and C). Compared with parent MFI crystals, MFI NSs exhibited an increased micropore surface area (table S1), which could be attributed to an enhanced crystallinity. To elucidate the necessity of calcination in the preparation of MFI NSs, here, we further subjected uncalcined parent MFI crystals to the same hydrothermal treatment conditions. It was observed that hydrothermal treatment led to the formation of leaf-like MFI crystals with considerable thickness; moreover, some MFI crystals were smashed into pieces (fig. S3). Therefore, calcination of parent MFI crystals before hydrothermal treatment was necessary. In addition, our research indicated that MFI NSs with desired morphology could be obtained only under a narrow range of hydrothermal treatment conditions. Sensitivity analysis indicated that even a slight variation in [TPAOH] (±0.015 M) or volume of solution (±0.5 g) would cause incomplete conversion of parent MFI crystals or structural disintegration of MFI NSs (figs. S4 and S5).

Besides 1.0-μm–sized MFI NSs, diverse regularly shaped parent MFI crystals with grain size ranging from 0.4 to 8.2 μm (fig. S6, A to C) were further synthesized to validate the generality of this wall-thinning strategy. As shown in Fig. 2 (G to I), uniform MFI NSs with grain size ranging from 0.3 to 7.5 μm were obtained after the adequate hydrothermal treatment of their parent ones. Our experiment indicated that the yields of 0.3-, 1.0-, 3.1-, and 7.5-μm–sized MFI NSs were 17, 15, 12, and 8%, respectively. Besides, XRD characterization further confirmed the phase purity of the resulting different-sized MFI NSs (fig. S6, D to F).

Substantial work has previously been conducted in the preparation of hollow MFI crystals by a dissolution-recrystallization mechanism in the presence of TPAOH (*27*, *28*). Briefly, at the early stage, parent zeolite cores were dissolved because of a relatively lower crystallinity. Subsequently, dissolved silica species were recrystallized on the outer surface of parent MFI crystals in the presence of TPA^+ cations. Since TPA^+ cations were too bulky to enter MFI pores, recrystallization occurred only on the outer surface; correspondingly, mesoscopic voids within MFI crystals generated by alkaline treatment were retained, leading to the formation of hollow hierarchical MFI crystals. In effect, we also observed the formation of hollow-structured MFI crystals (Fig. 3, A and B) during the formation process of MFI NSs, therefore demonstrating that morphological evolution of parent MFI crystals in the early stage followed the dissolution-recrystallization mechanism. Further prolonging the alkaline treatment time resulted in progressive thinning of zeolite walls in all directions (Fig. 3, C and D, and fig. S7, A and B). Last, only the largest faces arranged perpendicular to the *b*-axis of parent MFI crystals survived, leading to the formation of desired MFI NSs. Parent MFI crystals could be completely converted to MFI NSs, maintaining the structural integrity in case the hydrothermal treatment time varied between 12 hours (fig. S7C) and 18 hours (Fig. 2B). Nevertheless, prepared MFI NSs began to smash into pieces upon further extending the hydrothermal treatment time to 36 hours (fig. S7D). In addition, the reason why the thickness after hydrothermal treatment became ca. 25 nm could be ascribed to low stability of MFI NSs with thickness smaller than 25 nm (equivalent to 12 unit-cell thickness) as reported by Zhang *et al.* (*21*). Hydrothermal treatment of parent zeolite crystals led to progressive thinning of zeolite walls. As a result, only zeolite NSs with thickness around 25 nm along the *b*-axis could survive under prolonged hydrothermal treatment.

Considering the importance of maintaining the structural integrity of MFI NSs in layer processing, here, the mechanical robustness of MFI NSs was further evaluated by sonication and stirring. As shown in fig. S8, even after vigorous sonication (500 W) for 30 min or stirring (500 rpm) for 2 weeks, prepared MFI NSs maintained their structural integrity, which, as shown below, was the prerequisite for their oriented self-assembly.

Synthesis of MFI NSs seed monolayers

The second step involves oriented deposition of MFI NSs seed monolayers. Recently, we developed a DALIAS method for facile

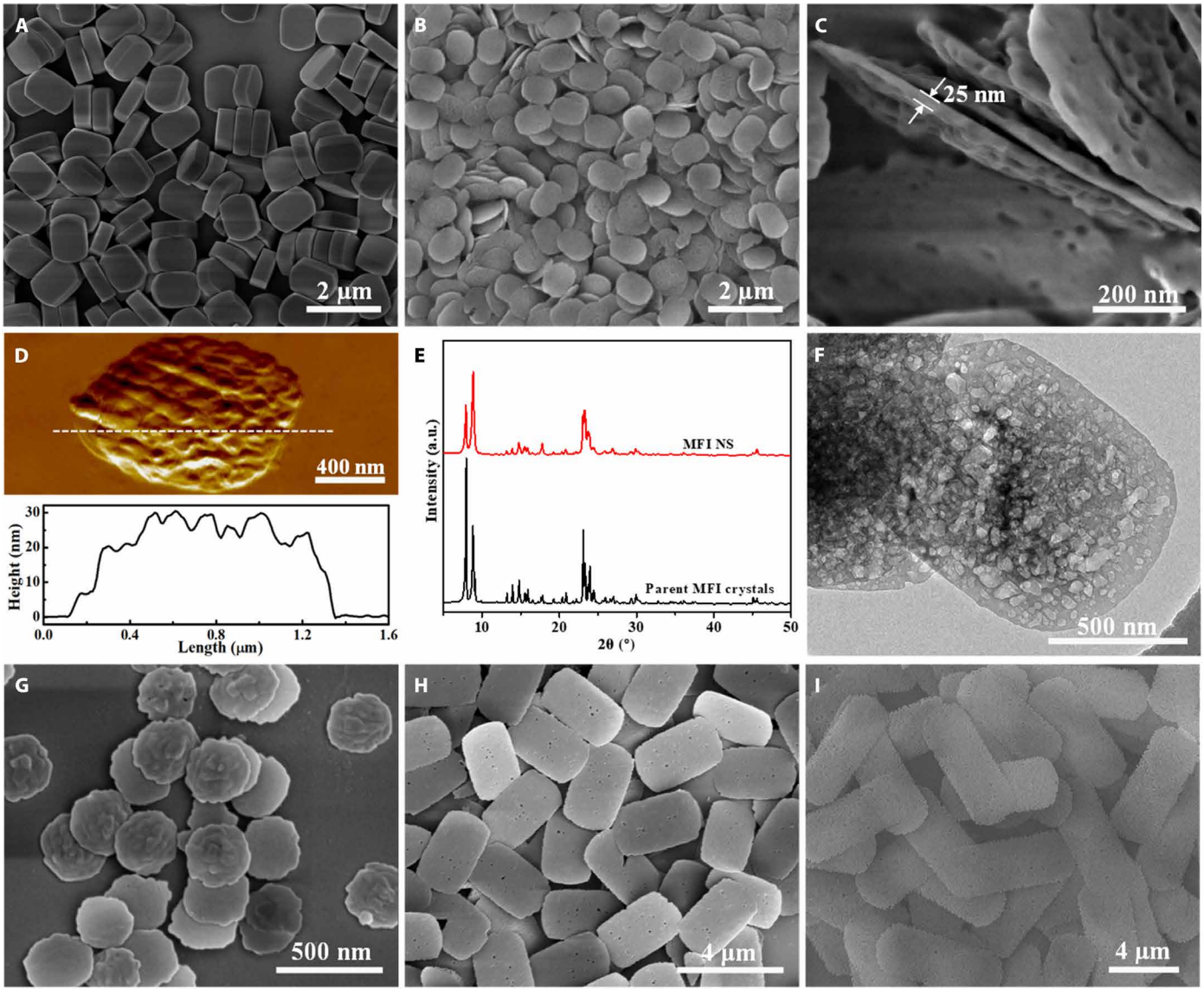

Fig. 2. Characterization of prepared MFI crystals and MFI NSs. (**A**) SEM images of 1.2-μm–sized parent MFI crystals. (**B** and **C**) SEM images, (**D**) AFM height image with a height profile along the indicated trace, (**E**) XRD patterns, and (**F**) TEM image of 1.0-μm–sized MFI NSs. SEM images of MFI NSs with sizes of (**G**) 0.3 μm, (**H**) 3.1 μm, and (**I**) 7.5 μm.

fabrication of highly *c*-oriented NH_2-MIL-125(Ti) monolayers (*29*). Here, this method was further used to organize MFI NSs into closely packed *b*-oriented seed monolayers. Briefly, 1.0-μm–sized MFI NSs were firstly uniformly dispersed in 2-butanol solution under vigorous stirring. Subsequently, the suspension was slowly injected to the turbulent air-water interface at which closely packed, highly *b*-oriented MFI NSs monolayers were formed (Fig. 4A). It was deemed that both geometric features of MFI NSs and the turbulent state at the air-liquid interface jointly improved the assembly quality and efficiency. Strong diffraction peaks derived from (0*k*0) planes further confirmed the dominance of *b*-orientation (Fig. 4D). Note that although this method also proved effective in *b*-oriented self-assembly of coffin-shaped parent MFI crystals (*14*, *17*, *30*), the use of MFI NSs as building blocks still exhibited noticeable superiorities in terms of efficiency, precision, simplicity, and generality. For instance, our research indicated that besides 2-butanol, dispersing MFI NSs in other alcohols (such as ethanol) also led to the formation of qualified monolayers (fig. S9A); moreover, it was no longer necessary to add any additives (such as linoleic acid) in the MFI NSs–containing suspension to ensure close contact between adjacent MFI NSs.

Besides the DALIAS method, we further tried to prepare closely packed *b*-oriented MFI NSs monolayers by manual rubbing (*31*), which has proven effective for oriented organization of coffin-shaped MFI crystals with decent aspect ratios. Nevertheless, this method was not adapted to MFI NSs self-assembly since substantial MFI NSs were smashed into pieces during this process (fig. S9B). It was anticipated that the DALIAS method described above could be generalized for oriented organization of other high–aspect ratio zeolite NSs relying on the mild operating condition.

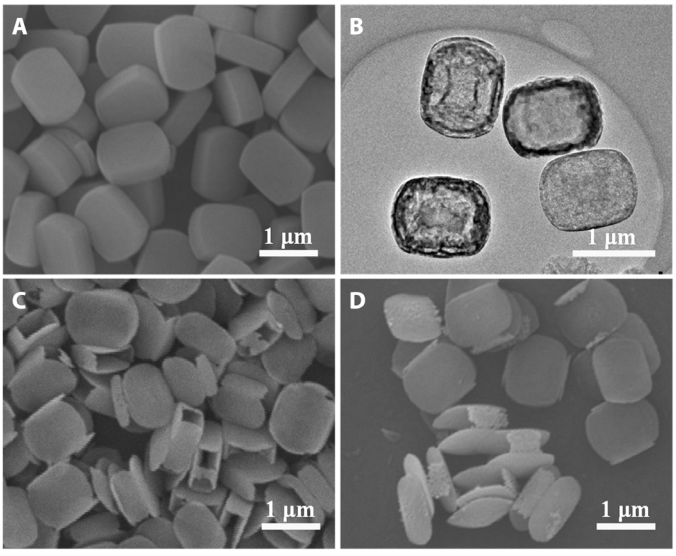

Fig. 3. SEM characterization of MFI NSs formation mechanism. (**A**) SEM image and (**B**) TEM image of MFI NSs prepared by alkaline treatment for 30 min. SEM images of MFI NSs prepared by alkaline treatment for (**C**) 40 min and (**D**) 60 min.

Synthesis of *b*-oriented ultrathin MFI layers

The third step involves in-plane epitaxial growth of *b*-oriented ultrathin MFI layers. So far, great efforts have been dedicated to suppression of twin growth of MFI layers during epitaixal growth process (*17*, *32*–*35*). In contrast, developing facile synthetic methods enabling precise control over layer thickness remained largely unexplored. It has been reported that twin-free *b*-oriented MFI layers with sub–100-nm thickness could be obtained by using the dry gel conversion (*20*, *36*) or gel-less method (*24*, *37*); nevertheless, it was unclear whether the commonly used solution-based epitaxial growth method could be used for fabricating sub–100-nm-thick *b*-oriented MFI layers.

Initially, a conventional hydrothermal method was used in this study for epitaxial growth of *b*-oriented MFI NSs monolayers under mild hydrothermal conditions. Nevertheless, our results showed that it was very difficult to prepare well-intergrown, sub–100-nm-thick *b*-oriented MFI layers by simple optimization of synthetic conditions (fig. S10, A to C). Alternatively, multimode microwave heating, which had proven quite effective in suppressing twin formation due to the unique nucleation bottleneck effect (*33*, *38*), was also used for MFI layer synthesis. Unfortunately, growth rate of MFI NSs seeds along the in-plane direction was too slow to warrant the formation of well-intergrown MFI layers even under optimized synthetic conditions (fig. S10D).

Instead of multimode microwave heating, in this study, single-mode microwave heating was further used in epitaxial growth of MFI NSs monolayers. It was anticipated that the in-plane growth rate of MFI NSs seeds could be remarkably enhanced, relying on the high field intensity and field homogeneity of single-mode microwave heating. Our results indicated that well-intergrown *b*-oriented MFI layers with few twin crystals (Fig. 4, B and D) were obtained by proper optimization of epitaxial growth conditions (fig. S11). The cross-sectional image further illustrated that prepared MFI layers were 93 nm thick (Fig. 4C). To the best of our knowledge, there has been rare report on sub–100-nm-thick MFI layer fabrication via solution-based epitaxial growth. Moreover, compared with the "dry gel" or "gel-less" conversion method, the reaction temperature required for the formation of well-intergrown MFI layers was much lower (100°C). In addition, single-mode microwave heating was used in the synthesis and microstructural optimization of zeolite layers. Relying on single-mode microwave heating, recently, we also successfully prepared 500-nm-thick *c*-oriented NH_2-MIL-125(Ti)–type MOF membranes with superior H_2/CO_2 selectivity (*29*). It was believed that single-mode microwave heating could serve as a powerful tool for molecular sieve layer processing.

Our concept was not only confined to smooth glass plates. By adopting this method, MFI NSs seed monolayers and ultrathin *b*-oriented MFI layers on coarse Al plates (Fig. 5, A and D), inert Pt electrodes (Fig. 5, B and E), and porous γ-Al_2O_3 substrates (Fig. 5, C and F) were sequentially prepared. Corresponding XRD patterns shown in fig. S12 indicated the dominance of *b* orientation for both MFI seed monolayers and MFI layers, while the appearance of diffraction peaks around 22° to 24° could be attributed to a much higher surface roughness of substrates as was confirmed by surface scanning electron microscope (SEM) images of Al plates, Pt electrodes, and porous γ-Al_2O_3 substrates (fig. S13). Consequently, their anti-corrosion capacity, ionic sieving property, and *n*-/*i*-butane isomer separation performance were systematically investigated, respectively. Initially, anticorrosion performance of MFI layer–coated Al plates was examined by direct current (DC) polarization. Corrosion current (I_{corr}) represented an effective parameter for direct evaluation of the performance of anticorrosion coatings (*39*, *40*). Our results (shown in Fig. 5G) indicated that I_{corr} for bare Al plates reached ~10^{-4} A cm^{-2}. After coating with *b*-oriented ultrathin MFI layers, a large decrease of I_{corr} to ~10^{-7} A cm^{-2} was achieved. The superior anticorrosion performance of MFI layer–modified Al plates could be attributed to smaller pore apertures (5.5 Å) compared with ionic radii of hydrated sodium cations (7.2 Å) and reduced defect density at grain boundaries. Consequently, we further verified ionic-sieving properties of *b*-oriented ultrathin MFI layers by fabricating onto Pt electrodes, which were then used as working electrodes in cyclic voltammetry experiments. Redox species of varying charge and size in aqueous solution, including $[Ru(NH_3)_6]^{3+}$ (~5.5 Å) and $[Fe(phen)_3]^{2+}$ (~13.0 Å), were tested. Since the pore aperture of MFI crystals along the *b* axis was 5.5 Å, in principle, $[Ru(NH_3)_6]^{3+}$ was able to pass through the MFI layer, while $[Fe(phen)_3]^{2+}$ would be excluded. As shown in Fig. 5 (H and I), compared with a bare Pt electrode, a weaker and deformed CV signal was detected for $[Ru(NH_3)_6]^{3+}$, while no CV response was found for $[Fe(phen)_3]^{2+}$ on MFI layer–modified electrodes. For a mixture of $[Ru(NH_3)_6]^{3+}$ and $[Fe(phen)_3]^{2+}$, only the redox signal for $[Ru(NH_3)_6]^{3+}$ was detected (Fig. 5J). All these results convincingly confirmed the precise ionic sieving through the *b* axis of MFI layers and the presence of few grain boundary defects. Last, gas separation performance of porous γ-Al_2O_3–supported MFI layers was evaluated by feeding equimolar *n*-/*i*-butane isomer mixtures through a Wicke-Kallenbach permeation cell (*41*). Our results indicated that, under optimized conditions, the selectivity for equimolar *n*-/*i*-butane isomer mixtures reached ~33 with an *n*-butane permeance of 2×10^{-7} mol m^{-2} s^{-1} Pa^{-1}, which was only slightly lower than the single gas permeance of *n*-butane through bare porous γ-Al_2O_3 substrates (5×10^{-7} mol m^{-2} s^{-1} Pa^{-1}). Obviously, the ultrathin MFI layer thickness contributed to a negligible mass transfer barrier. It was noted that the *n*-/*i*-butane isomer

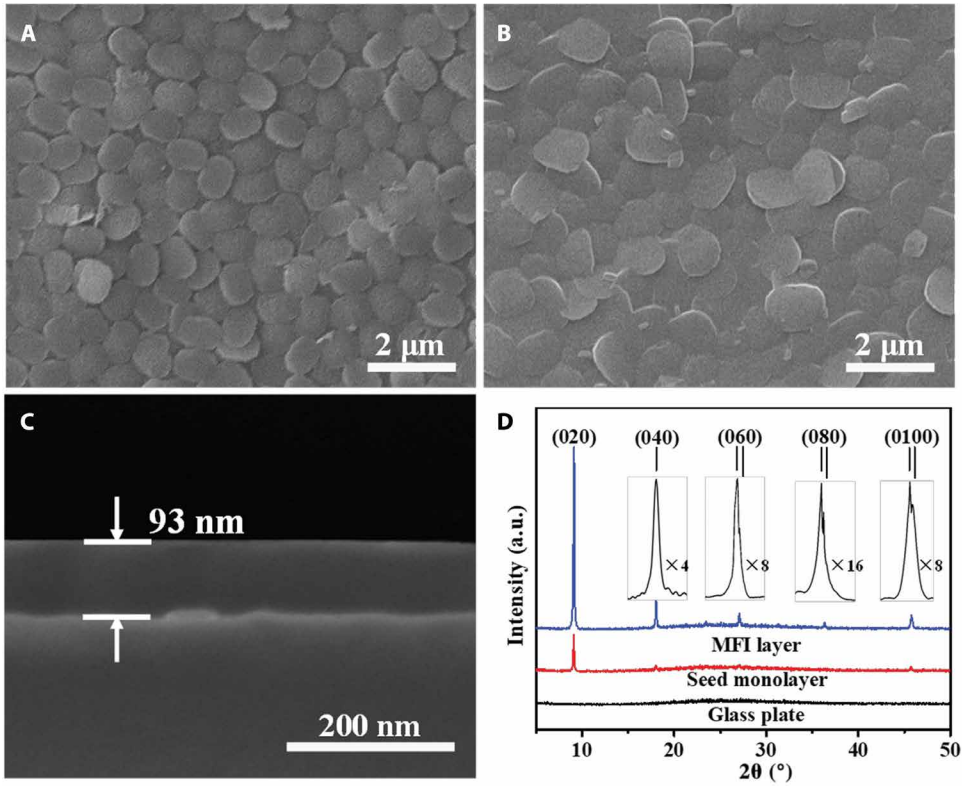

Fig. 4. Characterization of the prepared MFI seed monolayer and MFI layer. SEM images of (**A**) prepared MFI seed monolayer, (**B**) prepared MFI layer after secondary growth on glass plate, and its (**C**) cross-sectional image. (**D**) XRD patterns of glass plate, MFI seed monolayer, and the obtained MFI layer.

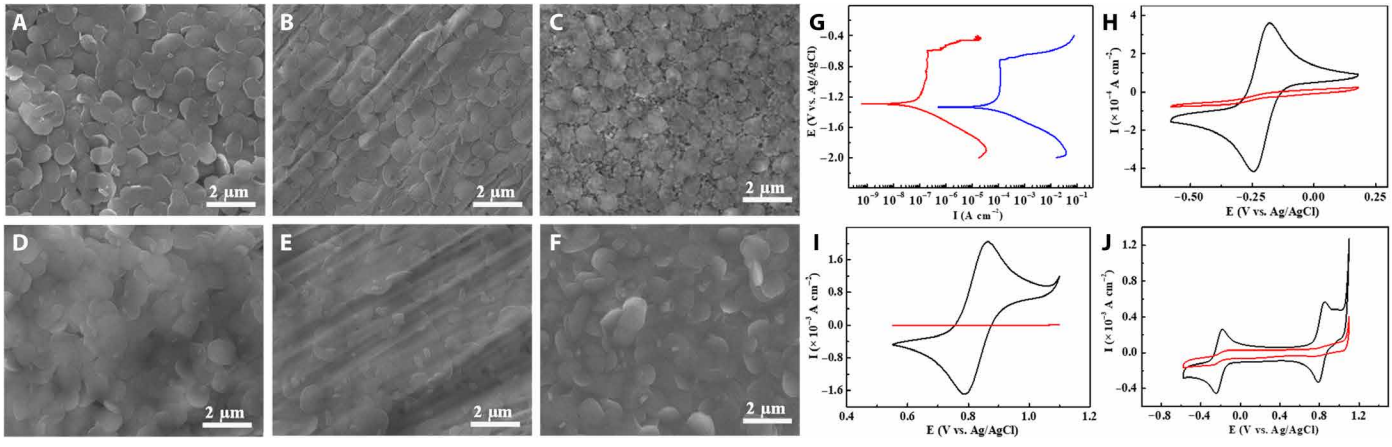

Fig. 5. SEM characterization and electrochemical test of the prepared MFI seed monolayers and MFI layers on different substrates. SEM images of surface morphologies of *b*-oriented MFI seed monolayers on (**A**) Al plates, (**B**) Pt electrodes, and (**C**) γ-Al_2O_3 substrates; *b*-oriented MFI layers after secondary growth (TPA gel composition, 1 TEOS:0.15 TPAOH:135 H_2O; 100°C; 120 min) on (**D**) Al plates, (**E**) Pt electrodes, and (**F**) γ-Al_2O_3 substrates. (**G**) DC polarization curves for bare (blue line) and *b*-oriented MFI layer–coated (red line) Al plates preincubated in 0.5 M NaCl solution for 30 min. Cyclic voltammograms of $[Ru(NH_3)_6]^{3+}$ and/or $[Fe(phen)_3]^{2+}$ in aqueous solutions. Black line, bare Pt electrode; red line, Pt electrode coated with *b*-oriented MFI layers for (**H**) $[Ru(NH_3)_6]^{3+}$, (**I**) $[Fe(phen)_3]^{2+}$, and (**J**) $[Ru(NH_3)_6]^{3+}$ + $[Fe(phen)_3]^{2+}$. Supporting electrolyte, 0.5 M KCl. Scan rate, 50 mV/s. Reference electrode, saturated Ag/AgCl electrode (SCE).

separation performance was superior to those of most MFI membranes hitherto reported (table S2). Last, to verify the reproducibility of this approach, we prepared and measured six membranes in parallel. Among them, relative SDs of *n*-butane permeance and *n*-/*i*-butane SF reached 14.2 and 7.7%, respectively (table S3), therefore indicating a high reproducibility of synthetic protocols. It should be emphasized that compared with *n*-/*i*-butane isomer separation, *p*-/*o*-xylene isomer separation should be a better indicator of MFI membrane quality. Unfortunately, *p*-/*o*-xylene isomer separation measurements could not be conducted owing to the limitation of current experiment conditions in our laboratory.

DISCUSSION

To summarize, in this study, we developed a facile approach involving anisotropic etching in an aqueous solution of TPAOH for preparation of ca. 12 unit-cell-thick hierarchical MFI zeolite NSs with high aspect ratios (ca. 40), which may achieve a better balance among stability, barrier, and processability. The mechanism involving MFI NSs formation was further discussed. Consequently, sub–100-nm-thick *b*-oriented MFI layers were successfully prepared by using the DALIAS method for oriented deposition of MFI NSs monolayers and single-mode microwave heating for controlled in-plane epitaxial growth. Electrochemical measurements (including DC polarization and cyclic voltammetry) and gas permeation tests indicated that prepared MFI layers exhibited superior anticorrosion capacity, ionic sieving property, and isomer separation performance. It is anticipated that the concept revealed in this work could bring some inspiration for microstructural optimization and performance improvement of diverse molecular sieve membranes.

MATERIALS AND METHODS

Materials and chemicals

Tetraethylorthosilicate (TEOS; 98%; Sinopharm Chemical Reagent Co., Ltd.), TPAOH (25% aqueous solution, Macklin), 2-butanol ($C_4H_{10}O$, 99%; Macklin), potassium chloride (KCl, 99.8%; Macklin), hexaammineruthenium(III) chloride ($[Ru(NH_3)_6]Cl_3$, 99%, Strem), and sodium chloride (NaCl, 99.5%; Macklin) were used without any further purification. $[Fe(phen)_3]Cl_2$ was synthesized in our laboratory, according to the well-documented procedure. Briefly, 0.994 g of iron(II) chloride tetrahydrate ($FeCl_2{\cdot}4H_2O$, 99.95%; Macklin) was dissolved in 250 ml of deionized (DI) water. Consequently, 2.97 g of 1,10-phenanthroline monohydrate ($C_{12}H_8N_2{\cdot}H_2O$, 98%; Macklin) was added into this aqueous solution. After vigorous stirring for 3 hours, $[Fe(phen)_3]Cl_2$ solution (20 mM) was prepared and stored in the dark before use. Glass plates (2 cm × 2 cm) were immerged in piranha solution (H_2SO_4/H_2O_2 = 2/1 v/v) and heated at 90°C for 1 hour, then washed with copious DI water, and stored in DI water before seed layer deposition. γ-Al_2O_3 discs (Fraunhofer IKTS, Germany) were pretreated with ~6% hydrochloric acid and extensively washed with water afterward. Pt electrodes (Shanghai Yueci Electronic Technology Co., Ltd) and Al plates were polished with sandpapers, thoroughly washed with ethanol, and stored in DI water before deposition.

Methods

Preparation of parent MFI crystals with different grain sizes

MFI seed crystals with different grain sizes were synthesized from a gel composed of TEOS, TPAOH, and DI water. The synthesis gel was prepared by introducing TEOS into aqueous solutions containing TPAOH. After stirring for 4 hours at room temperature, the mixture was transformed into clear gel and then poured into a Teflon-lined stainless-steel autoclave. The autoclave was placed in a rotational convection oven (60 r/min) at an assigned temperature (*T*) for a certain time (*t*). Afterward, resulting solid products were centrifuged, washed with distilled water, and dried at 70°C in an oven overnight. Last, calcination was conducted at 550°C for 6 hours. A summary of detailed synthetic conditions is shown in table S4.

Preparation of MFI NSs with different grain sizes

For 0.3-μm–sized MFI NSs, 0.1 g of calcined 0.4-μm–sized parent MFI crystals was added in 15.5 g of 0.12 M TPAOH solution [1 MFI (SiO_2-based):1.12 TPAOH:505 H_2O]. For 1.0-μm–sized MFI NSs, 0.2 g of calcined 1.2-μm–sized parent MFI crystals was added in 16.5 g of 0.217 M TPAOH solution [1 MFI (SiO_2-based):1.08 TPAOH:263 H_2O]. For 3.1-μm–sized MFI NSs, 0.2 g of calcined 3.5-μm–sized parent MFI crystals was added in 15 g of 0.23 M TPAOH solution [1 MFI (SiO_2-based):1.04 TPAOH:241 H_2O]. For 7.5-μm–sized MFI NSs, 0.2 g of calcined 8.2-μm–sized parent MFI crystals was added in 15 g of 0.24 M TPAOH solution [1 MFI (SiO_2-based):1.08 TPAOH:238 H_2O]. Prepared suspension was then transferred into a Teflon-lined stainless-steel autoclave. Hydrothermal treatment was carried out at 170°C for 18 hours in a rotational convection oven (60 r/min). Obtained solid precipitates were recovered by centrifugation and dried overnight at 70°C.

Preparation of b-oriented MFI seed monolayer

Before seed deposition, 0.005 g of MFI NSs was dispersed with 4 ml of 2-butanol and stirred unceasingly for 2 days to form a homogeneous zeolite suspension. Afterward, a glass plate (2 cm × 2 cm) was placed horizontally below the water, and the zeolite suspension was slowly and continuously injected at the turbulent air-water interface at a speed of 3 μl·min^{-1}. After an elapsed time of 12 min, a closely packed and highly *b*-oriented MFI NSs monolayer was formed at the air-liquid interface and then transferred to the glass plate. Last, structure-directing agent (SDA) plugged in the seed layer was removed by calcination at 550°C for 6 hours. The procedure for deposition of MFI NSs monolayers on other substrates was the same as mentioned above.

Preparation of ultrathin b-oriented MFI layers

Single-mode microwave heating was used for epitaxial growth of MFI NSs monolayers following the procedure shown below: First, the precursor solution was prepared by adding 2 g of TEOS dropwise into the solution containing 1.171 g of TPAOH and 22.45 g of DI water. The precursor solution became clear after vigorous stirring for 4 hours at room temperature. Second, MFI NSs monolayer–coated substrates were placed vertically in an 80-ml glass vessel prefilled with 30 ml of clear precursor solution. Third, the vessel was sealed and heated in a single-mode microwave oven (Discover, CEM) at 100°C for 120 min. After cooling to room temperature, the MFI layer was further rinsed in a 0.1 M ammonia solution overnight. Fourth, calcination was conducted at 500°C for 6 hours with a heating rate of 0.2°C·min^{-1} and a cooling rate of 0.3°C·min^{-1}. Multimode microwave heating (CEM Mars 6) was used for epitaxial growth of MFI NSs monolayers with the same synthetic conditions as single-mode heating.

Conventional convection heating was used for epitaxial growth of MFI NSs monolayers with the same synthetic conditions as single-mode heating except that hydrothermal reaction was conducted at 100°C for 6 hours in a convective oven preheated to 100°C. A summary of detailed synthetic conditions is shown in table S5.

Characterization

XRD patterns were recorded on a Rigaku SmartLab diffractometer using Cu Kα radiation (λ = 1.5418 Å) at 45 kV, 200 mA. The spectra were recorded over a 2θ range of 5° to 50° with a step size of 0.02°. SEM images were obtained on a field-emission scanning electron microscope (NOVA NanoSEM 450) with an acceleration voltage of 3 kV. TEM images were taken on a JEM-2100 instrument (JEOL Company) with an acceleration voltage of 200 kV. N_2 adsorption-desorption isotherms at 77 K were measured using a Mike ASAP 2020 Plus gas adsorption analyzer. The BET method was applied to calculate the total surface area, and the *t*-plot method was used to

calculate the microporous surface area. The micropore distributions were calculated according to the SF method and the mesopore distributions were converted from the entire adsorption branch according to the Barrett-Joyner-Halenda algorithm for approximation. AFM images were obtained on a PicoScan 2500 instrument (MI Company). Electrochemical data were obtained using a CHI660E electrochemical workstation with computer data acquisition and control.

Electrochemical tests

Cyclic voltammetry experiments were performed in aqueous solutions with 0.5 M KCl as supporting electrolyte. CV responses of $[Ru(NH_3)_6]^{3+}$ and $[Fe(phen)_3]^{2+}$ were obtained with a concentration of 3 and 20 mM, respectively. For a mixture of $[Ru(NH_3)_6]^{3+}$ and $[Fe(phen)_3]^{2+}$, concentrations were adjusted to 3 and 5 mM, respectively. DC polarization tests were performed in corrosive mediums of 0.5 M NaCl aqueous solution. Before the test, samples were immersed in a corrosive medium to measure the open circuit potential. The sweep rate and potential range of DC polarization test were set at −2.0 to −0.4 V (versus reference) and 10 mV/s, respectively. Electrochemical experiments were conducted at room temperature (25°C) with a conventional three-electrode setup with an MFI layer–coated Pt electrode as the working electrode, a Pt wire as the counter electrode, and a saturated Ag/AgCl electrode as the reference electrode. MFI layer–coated Pt electrodes were immersed in the test solution for 30 min before the electrochemical test.

Gas permeation test

Prepared γ-Al_2O_3–supported MFI layer was fixed in a module sealed with O-rings. Ar (50 ml·min^{-1}) was used as the sweep gas. For the mixed gas permeation measurement, both feed and sweep flow rates were set to 50 ml·min^{-1}, while the pressure at both sides was kept at 1 bar. A calibrated gas chromatograph (GC7900 TECHCOMP) was used to measure the concentration of mixed gases on the permeate side. The separation factor $\alpha_{i,j}$ of a binary mixture is defined as the quotient of the molar ratios of the components (*i*,*j*) in the permeate divided by the quotient of the molar ratio of the components (*i*,*j*) in the feed

$$\alpha_{i,j} = \frac{X_{i,\mathrm{perm}}/X_{j,\mathrm{perm}}}{X_{i,\mathrm{feed}}/X_{j,\mathrm{feed}}}$$

SUPPLEMENTARY MATERIALS

Supplementary material for this article is available at http://advances.sciencemag.org/cgi/content/full/6/7/eaay5993/DC1

Fig. S1. Experimental and simulated electron diffraction (ED) patterns of 1.0-μm–sized MFI NSs.
Fig. S2. N_2 physical adsorption characterization of 1.0-μm–sized MFI NSs and corresponding parent MFI crystals.
Fig. S3. Influence of organic template removal on final morphology of MFI particles.
Fig. S4. Influence of [TPAOH] on final morphology of MFI NSs.
Fig. S5. Influence of the volume of TPAOH solution on final morphology of MFI NSs.
Fig. S6. Characterization of parent MFI crystals and MFI NSs with different sizes.
Fig. S7. Influence of hydrothermal treatment time on final morphology of MFI NSs.
Fig. S8. Mechanical robustness test of 1.0-μm–sized MFI NSs.
Fig. S9. SEM characterization of MFI seed monolayers assembled with ethanol and obtained by manual rubbing.
Fig. S10. SEM characterization of MFI layers prepared by conventional convective heating and multi-mode microwave heating.
Fig. S11. SEM characterization of MFI layers prepared by single-mode microwave heating.
Fig. S12. XRD characterization of *b*-oriented MFI seed monolayers and *b*-oriented MFI layers on different substrates.
Fig. S13. SEM characterization of the surface morphology of Al plate, Pt electrode, and porous γ-Al_2O_3 substrate.
Table S1. Textural properties of 1.0-μm–sized MFI NSs and the corresponding parent MFI crystals.
Table S2. A summary of the separation performance of reported MFI membranes for butane isomer mixture separation in the temperature range of 22° to 30°C.
Table S3. Reproducibility of γ-Al_2O_3–supported ultrathin *b*-oriented MFI layers.
Table S4. A summary of synthetic conditions of parent MFI crystals.
Table S5. A summary of synthetic conditions of MFI layers on glass plates.
References (*42*–*59*)

REFERENCES AND NOTES

1. M. Choi, K. Na, J. Kim, Y. Sakamoto, O. Terasaki, R. Ryoo, Stable single-unit-cell nanosheets of zeolite MFI as active and long-lived catalysts. *Nature* **461**, 246–249 (2009).
2. M. Tsapatsis, 2–Dimensional zeolites. *AIChE J.* **60**, 2374–2381 (2014).
3. K. Na, C. Jo, J. Kim, W.-S. Ahn, R. Ryoo, MFI titanosilicate nanosheets with single-unit-cell thickness as an oxidation catalyst using peroxides. *ACS Catal.* **1**, 901–907 (2011).
4. P. Kumar, K. V. Agrawal, M. Tsapatsis, K. A. Mkhoyan, Quantification of thickness and wrinkling of exfoliated two-dimensional zeolite nanosheets. *Nat. Commun.* **6**, 7128–7134 (2015).
5. N. Rangnekar, N. Mittal, B. Elyassi, J. Caro, M. Tsapatsis, Zeolite membranes—A review and comparison with MOFs. *Chem. Soc. Rev.* **44**, 7128–7154 (2015).
6. K. Varoon, X. Zhang, B. Elyassi, D. D. Brewer, M. Gettel, S. Kumar, J. A. Lee, S. Maheshwari, A. Mittal, C.-Y. Sung, M. Cococcioni, L. F. Francis, A. V. McCormick, K. A. Mkhoyan, M. Tsapatsis, Dispersible exfoliated zeolite nanosheets and their application as a selective membrane. *Science* **334**, 72–75 (2011).
7. M. Y. Jeon, D. Kim, P. Kumar, P. S. Lee, N. Rangnekar, P. Bai, M. Shete, B. Elyassi, H. S. Lee, K. Narasimharao, S. N. Basahel, S. Al-Thabaiti, W. Xu, H. J. Cho, E. O. Fetisov, R. Thyagarajan, R. F. DeJaco, W. Fan, K. A. Mkhoyan, J. I. Siepmann, M. Tsapatsis, Ultra-selective high-flux membranes from directly synthesized zeolite nanosheets. *Nature* **543**, 690–694 (2017).
8. Z. Cao, S. Zeng, Z. Xu, A. Arvanitis, S. Yang, X. Gu, J. Dong, Ultrathin ZSM-5 zeolite nanosheet laminated membrane for high-flux desalination of concentrated brines. *Sci. Adv.* **4**, eaau8634 (2018).
9. H. Zhang, Q. Xiao, X. Guo, N. Li, P. Kumar, N. Rangnekar, M. Y. Jeon, S. Al-Thabaiti, K. Narasimharao, S. N. Basahel, B. Topuz, F. J. Onorato, C. W. Macosko, K. A. Mkhoyan, M. Tsapatsis, Open-pore two-dimensional MFI zeolite nanosheets for the fabrication of hydrocarbon-isomer-selective membranes on porous polymer supports. *Angew. Chem. Int. Ed.* **55**, 7184–7187 (2016).
10. B. Min, S. Yang, A. Korde, Y. H. Kwon, C. W. Jones, S. Nair, Continuous zeolite MFI membranes fabricated from 2D MFI nanosheets on ceramic hollow fibers. *Angew. Chem. Int. Ed.* **58**, 8201–8205 (2019).
11. Z. Lai, G. Bonilla, I. Diaz, J. G. Nery, K. Sujaoti, M. A. Amat, E. Kokkoli, O. Terasaki, R. W. Thompson, M. Tsapatsis, D. G. Vlachos, Microstructural optimization of a zeolite membrane for organic vapor separation. *Science* **300**, 456–460 (2003).
12. G. Bonilla, I. Díaz, M. Tsapatsis, H.-K. Jeong, Y. Lee, D. G. Vlachos, Zeolite (MFI) crystal morphology control using organic structure-directing agents. *Chem. Mater.* **16**, 5697–5705 (2004).
13. K. B. Yoon, Organization of zeolite microcrystals for production of functional materials. *Acc. Chem. Res.* **40**, 29–40 (2007).
14. Y. Liu, Y. Li, W. Yang, Fabrication of highly *b*-oriented MFI monolayers on various substrates. *Chem. Commun.* , 1520–1522 (2009).
15. D. Kim, M. Y. Jeon, B. L. Stottrup, M. Tsapatsis, para-Xylene ultra-selective zeolite MFI membranes fabricated from nanosheet monolayers at the air–water interface. *Angew. Chem. Int. Ed.* **57**, 480–485 (2018).
16. T. C. T. Pham, H. S. Kim, K. B. Yoon, Growth of uniformly oriented silica MFI and BEA zeolite films on substrates. *Science* **334**, 1533–1538 (2011).
17. Y. Liu, Y. Li, W. Yang, Fabrication of highly *b*-oriented MFI film with molecular sieving properties by controlled in-plane secondary growth. *J. Am. Chem. Soc.* **132**, 1768–1769 (2010).
18. M. Shete, M. Kumar, D. H. Kim, N. Rangnekar, D. Xu, B. Topuz, K. V. Agrawal, E. Karapetrova, B. Stottrup, S. Al-Thabaiti, S. Basahel, K. Narasimharao, J. D. Rimer, M. Tsapatsis, Nanoscale control of homoepitaxial growth on a two-dimensional zeolite. *Angew. Chem. Int. Ed.* **56**, 535–539 (2017).
19. K. Agrawal, B. Topuz, Z. Jiang, K. Nguenkam, B. Elyassi, L. F. Fran-cis, M. Tsapatsis, M. Navarro, Solution-processable exfoliated zeolite nanosheets purified by density gradient centrifugation. *AIChE J.* **59**, 3458–3467 (2013).
20. M. Zhou, J. Hedlund, Facile preparation of hydrophobic colloidal MFI and CHA crystals and oriented ultrathin films. *Angew. Chem. Int. Ed.* **57**, 10966–10970 (2018).
21. F. Zhang, Y. Liu, Q. Sun, Z. Dai, H. Gies, Q. Wu, S. Pan, C. Bian, Z. Tian, X. Meng, Y. Zhang, X. Zou, X. Yi, A. Zheng, L. Wang, F.-S. Xiao, Design and preparation of efficient

hydroisomerization catalysts by the formation of stable SAPO-11 molecular sieve nanosheets with 10–20 nm thickness and partially blocked acidic sites. *Chem. Commun.* **53**, 4942–4945 (2017).
22. Z. Lai, M. Tsapatsis, J. P. Nicolich, Siliceous ZSM-5 membrane by secondary growth of *b*-oriented seed layers. *Adv. Fun. Mater.* **14**, 716–729 (2004).
23. N. Rangnekar, M. Shete, K. V. Agrawal, B. Topuz, P. Kumar, Q. Guo, I. Ismail, A. Alyoubi, S. Basahel, K. Narasimharao, C. W. Macosko, K. A. Mkhoyan, S. Al-Thabaiti, B. Stottrup, M. Tsapatsis, 2D zeolite coatings: Langmuir-schaefer deposition of 3 nm thick MFI zeolite nanosheets. *Angew. Chem. Int. Ed.* **54**, 6571–6575 (2015).
24. K. V. Agrawal, B. Topuz, T. C. T. Pham, T. H. Nguyen, N. Sauer, N. Rangnekar, H. Zhang, K. Narasimharao, S. N. Basahel, L. F. Francis, C. W. Macosko, S. Al-Thabaiti, M. Tsapatsis, K. B. Yoon, Oriented MFI membranes by gel-less secondary growth of sub-100 nm MFI-nanosheet seed layers. *Adv. Mater.* **27**, 3243–3249 (2015).
25. D. Kim, M. Shete, M. Tsapatsis, Large-grain, oriented, and thin zeolite MFI films from directly synthesized nanosheet coatings. *Chem. Mater.* **30**, 3545–3551 (2018).
26. Y. Dong, Y. Peng, G. Wang, Z. Wang, Y. Yan, Corrosion-resistant zeolite silicalite-1 coatings synthesized by seeded growth. *Ind. Eng. Chem. Res.* **51**, 3646–3652 (2012).
27. C. Dai, A. Zhang, L. Li, K. Hou, F. Ding, J. Li, D. Mu, C. Song, M. Liu, X. Guo, Synthesis of hollow nanocubes and macroporous monoliths of silicalite-1 by alkaline treatment. *Chem. Mater.* **25**, 4197–4205 (2013).
28. C. Pagis, A. R. Morgado Prates, D. Farrusseng, N. Bats, A. Tuel, Hollow zeolite structures: An overview of synthesis methods. *Chem. Mater.* **28**, 5205–5223 (2016).
29. Y. Sun, Y. Liu, J. Caro, X. Guo, C. Song, Y. Liu, In-plane epitaxial growth of highly *c*-oriented NH_2-MIL-125(Ti) membranes with superior H_2/CO_2 selectivity. *Angew. Chem. Int. Ed.* **57**, 16088–16093 (2018).
30. Y. Liu, Y. Li, W. Yang, Phase-segregation-induced self-assembly of anisotropic MFI microbuilding blocks into compact and highly *b*-oriented monolayers. *Langmuir* **27**, 2327–2333 (2011).
31. J. S. Lee, J. H. Kim, Y. J. Lee, N. C. Jeong, K. B. Yoon, Manual assembly of microcrystal monolayers on substrates. *Angew. Chem. Int. Ed.* **46**, 3087–3090 (2007).
32. X. Lu, Y. Peng, Z. Wang, Y. Yan, Rapid fabrication of highly *b*-oriented zeolite MFI thin films using ammonium salts as crystallization-mediating agents. *Chem. Commun.* **51**, 11076–11079 (2015).
33. Y. Liu, Y. Li, R. Cai, W. Yang, Suppression of twins in *b*-oriented MFI molecular sieve films under microwave irradiation. *Chem. Commun.* **48**, 6782–6784 (2012).
34. X. Li, Y. Peng, Z. Wang, Y. Yan, Synthesis of highly *b*-oriented zeolite MFI films by suppressing twin crystal growth during the secondary growth. *CrstEngComm* **13**, 3657–3660 (2011).
35. Y. Peng, X. Lu, Z. Wang, Y. Yan, Fabrication of *b*-oriented MFI zeolite films under neutral conditions without the use of hydrogen fluoride. *Angew. Chem. Int. Ed.* **127**, 5801–5804 (2015).
36. X. Lu, Y. Yang, J. Zhang, Y. Yan, Z. Wang, Solvent-free secondary growth of highly *b*-oriented MFI zeolite films from anhydrous synthetic powder. *J. Am. Chem. Soc.* **141**, 2916–2919 (2019).
37. T. C. T. Pham, T. H. Nguyen, K. B. Yoon, Gel-free secondary growth of uniformly oriented silica MFI zeolite films and application for xylene separation. *Angew. Chem. Int. Ed.* **52**, 8693–8698 (2013).
38. X. Li, Y. Yan, Z. Wang, Continuity control of *b*-oriented MFI zeolite films by microwave synthesis. *Ind. Eng. Chem. Res.* **49**, 5933–5938 (2010).
39. F. Mansfeld, Tafel slopes and corrosion rates obtained in the pre-Tafel region of polarization curves. *Corros. Sci.* **47**, 3178–3186 (2005).
40. H. J. Flitt, D. P. Schweinsberg, A guide to polarization curve interpretation: Deconstruction of experimental curves typical of the $Fe/H_2O/H^+/O_2$ corrosion system. *Corros. Sci.* **47**, 2125–2156 (2005).
41. Q. Wang, A. Wu, S. Zhong, B. Wang, R. Zhou, Highly (*h*0*h*)-oriented silicalite-1 membranes for butane isomer separation. *J. Membr. Sci.* **540**, 50–59 (2017).
42. K. Keizer, A. J. Burggraaf, Z. A. E. P. Vroon, H. Verweij, Two component permeation through thin zeolite MFI membranes. *J. Membr. Sci.* **147**, 159–172 (1998).
43. S. Alfaro, M. Arruebo, J. Coronas, M. Menéndez, J. Santamaría, Preparation of MFI type tubular membranes by steam-assisted crystallization. *Microporous Mesoporous Mater.* **50**, 195–200 (2001).
44. J. Choi, S. Ghosh, L. King, M. Tsapatsis, MFI zeolite membranes from a- and randomly oriented monolayers. *Adsorption* **12**, 339–360 (2006).
45. J. Choi, H.-K. Jeong, M. A. Snyder, J. A. Stoeger, R. I. Masel, M. Tsapatsis, Grain boundary defect elimination in a zeolite membrane by rapid thermal processing. *Science* **325**, 590–593 (2009).
46. L. Gora, J. C. Jansen, T. Maschmeyer, Controlling the performance of silicalite-1 membranes. *Chem. A Eur. J.* **6**, 2537–2543 (2000).
47. L. Gora, N. Nishiyama, J. C. Jansen, F. Kapteijn, V. Teplyakov, T. Maschmeyer, Highly reproducible high-flux silicalite-1 membranes: Optimization of silicalite-1 membrane preparation. *Sep. Purif. Technol.* **22–23**, 223–229 (2001).
48. L. Gora, J. C. Jansen, Hydroisomerization of C_6 with a zeolite membrane reactor. *J. Catal.* **230**, 269–281 (2005).
49. J. Hedlund, J. Sterte, M. Anthonis, A.-J. Bons, B. Carstensen, N. Corcoran, D. Cox, H. Deckman, W. D. Gijnst, P.-P. de Moor, F. Lai, J. McHenry, W. Mortier, J. Reinoso, J. Peters, High-flux MFI membranes. *Microporous Mesoporous Mater.* **52**, 179–189 (2002).
50. G. Xomeritakis, A. Gouzinis, S. Nair, T. Okubo, M. He, R. M. Overney, M. Tsapatsis, Growth, microstructure, and permeation properties of supported zeolite (MFI) films and membranes prepared by secondary growth. *Chem. Eng. Sci.* **54**, 3521–3531 (1999).
51. G. Xomeritakis, S. Nair, M. Tsapatsis, Transport properties of alumina-supported MFI membranes made by secondary (seeded) growth. *Microporous Mesoporous Mater.* **38**, 61–73 (2000).
52. Z. A. E. P. Vroon, K. Keizer, M. J. Gilde, H. Verweij, A. J. Burggraaf, Transport properties of alkanes through ceramic thin zeolite MFI membranes. *J. Membr. Sci.* **113**, 293–300 (1996).
53. J. M. van de Graaf, E. van der Bijl, A. Stol, F. Kapteijn, J. A. Moulijn, Effect of operating conditions and membrane quality on the separation performance of composite silicalite-1 membranes. *Ind. Eng. Chem. Res.* **37**, 4071–4083 (1998).
54. N. Nishiyama, L. Gora, V. Teplyakov, F. Kapteijn, J. A. Moulijn, Evaluation of reproducible high flux silicalite-1 membranes: Gas permeation and separation characterization. *Sep. Purif. Technol.* **22–23**, 295–307 (2001).
55. F. Jareman, J. Hedlund, J. Sterte, Effects of aluminum content on the separation properties of MFI membranes. *Sep. Purif. Technol.* **32**, 159–163 (2003).
56. Y. Li, X. Zhang, J. Wang, Preparation for ZSM-5 membranes by a two-stage varying-temperature synthesis. *Sep. Purif. Technol.* **25**, 459–466 (2001).
57. T. Matsufuji, N. Nishiyama, M. Matsukata, K. Ueyama, Separation of butane and xylene isomers with MFI-type zeolitic membrane synthesized by a vapor-phase transport method. *J. Membr. Sci.* **178**, 25–34 (2000).
58. J. A. Stoeger, J. Choi, M. Tsapatsis, Rapid thermal processing and separation performance of columnar MFI membranes on porous stainless steel tubes. *Energ. Environ. Sci.* **4**, 3479–3486 (2011).
59. A. Wu, C. Tang, S. Zhong, B. Wang, J. Zhou, R. Zhou, Synthesis optimization of (*h* 0 *h*)-oriented silicalite-1 membranes for butane isomer separation. *Sep. Purif. Technol.* **214**, 51–60 (2019).

Acknowledgments: We appreciate the technical support from Tencomp High-Tech Instrument Corporation (Peking) and Hitachi Ltd. for high-resolution SEM characterization of MFI NSs samples (Regulus 8100). **Funding:** We thank the National Natural Science Foundation of China (21176231); the Thousand Youth Talents Program, Liaoning Revitalization Talents Program (XLYC1807084); and the Technology Innovation Team of Dalian University of Technology (DUT2017TB01) for financial support. **Author contributions:** Y.L.* and Y.L. conceived the idea and designed the experiments. Y.L. performed experiments and analyzed the data. W.Q. assisted in diagram drawing, proofreading, and characterization data arrangement. T.J. and M.Z. helped with the electrochemical test. M.L. provided simulated electron diffraction patterns along with the corresponding zone axis. J.L. gave advice and helped analyze the characterization data. Y.L.* and Y.L. co-wrote the manuscript with contributions from all authors. **Competing interests:** The authors declare that they have no competing interests. **Data and materials availability:** All data needed to evaluate the conclusions in the paper are present in the paper and/or the Supplementary Materials. Additional data related to this paper may be requested from the authors.

Submitted 2 July 2019
Accepted 25 November 2019
Published 14 February 2020
10.1126/sciadv.aay5993

Citation: Y. Liu, W. Qiang, T. Ji, M. Zhang, M. Li, J. Lu, Y. Liu, Uniform hierarchical MFI nanosheets prepared via anisotropic etching for solution-based sub–100-nm-thick oriented MFI layer fabrication. *Sci. Adv.* **6**, eaay5993 (2020).